J. Fluid Mech. (2021), *vol*. 920, A8, doi:10.1017/jfm.2021.418

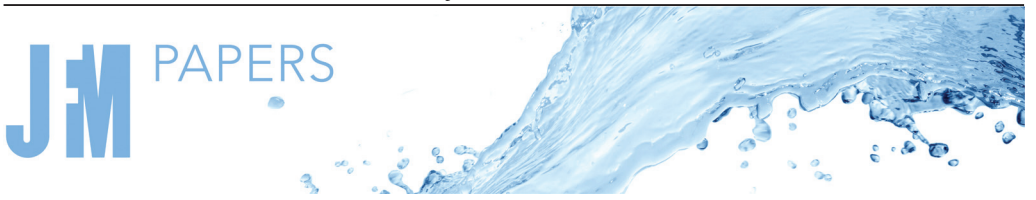

The exchanges between the mainstream in an open channel and a recirculating flow on its side at large Froude numbers

Shooka Karimpour[1,†], **Tao Wang**[2] **and Vincent H. Chu**[2]

[1]Department of Civil Engineering, York University, Toronto, ON M3J 1P3, Canada

[2]Department of Civil Engineering and Applied Mechanics, McGill University, Montreal, QC H3A 0C3, Canada

(Received 12 July 2020; revised 5 May 2021; accepted 6 May 2021)

The exchange of tracer mass in shallow waters between the mainstream and a recirculating flow to the side is examined in this paper over a wider range of Froude numbers than in any previous studies. We used a well-calibrated weighted essentially non-oscillatory scheme to capture the shock waves while maintaining the stability of the computation. The radiation of the waves suppressed the turbulence and the entrainment of surrounding fluids into a mixing layer. Shock waves began to form in the recirculating flow at a mainstream Froude number of $Fr_o \simeq 3$. The effect of the shock waves was a sudden increase in lateral mixing between the mainstream and the recirculating flow, leading to a corresponding sharp drop in a retention-time coefficient. These simulation results for the effect of the waves on mixing in shallow waters at large Froude numbers were consistent with the available data obtained from laboratory experiments.

Key words: channel flow, wave–turbulence interactions, turbulent mixing

1. Introduction

The lateral exchange between a fast moving current and a slower recirculating flow on the side is often encountered in the design of man-made waterways and in the training of natural rivers (Shields, Cooper & Knight 1995; Uijttewaal, Lehmann & van Mazijk 2001). The sedimentation and vegetation in the low-flow areas along the shore are affected by turbulence and waves. Many laboratory experiments were conducted to study the exchanges between the mainstream and the recirculating flow on the side. Most of the existing studies were for sub-critical flow with the value of the Froude number well below unity (Alavian & Chu 1985; Babarutsi, Ganoulis & Chu 1989; Booij 1989;

† Email address for correspondence: Shooka.Karimpour@lassonde.yorku.ca

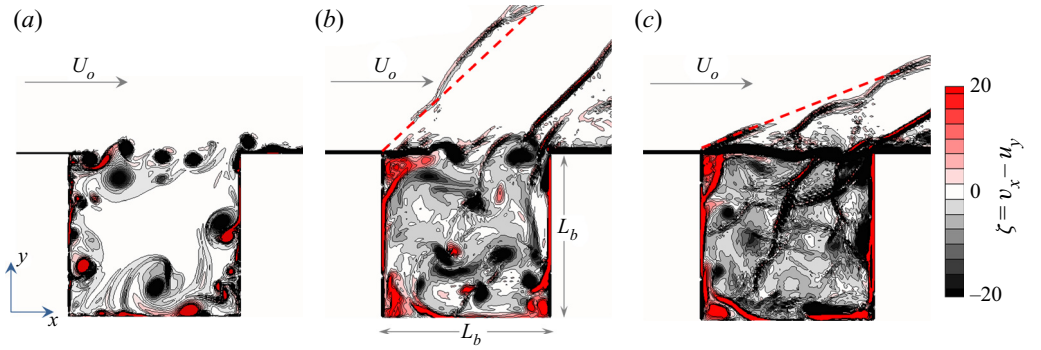

Figure 1. The exchange processes between the mainstream in a shallow open-channel flow and the recirculating flow in a square basin. The profiles of the vorticity, $\zeta = \frac{\partial v}{\partial x} - \frac{\partial u}{\partial y}$, on the horizontal x–y plane depict the exchanges for three different mainstream Froude numbers of (*a*) $Fr_o = 0.2$, (*b*) $Fr_o = 1.5$ and (*c*) $Fr_o = 3.0$. The red dashed lines in (*b*,*c*) mark the 'Froude line' with an oblique angle of $\theta = \sin^{-1}(1/Fr_o)$.

Uijttewaal 2005; Van Prooijen, Battjes & Uijttewaal 2005; Xiang *et al.* 2020; Yossef & de Vriend 2010). Numerical simulations have also been conducted for sub-critical flow of low Froude number using the rigid-lid approximation (McCoy, Constantinescu & Weber 2008; Xiang *et al.* 2020). However, the flow in rivers is often super-critical during flooding events (Petaccia *et al.* 2013; Kvočka, Ahmadian & Falconer 2017). These super-critical flows with large Froude numbers are not describable by the conventional theory of turbulence. The waves have a prominent role but their effect on turbulent mixing is not well understood.

To study the role of waves, we conducted numerical simulations for the exchange between a recirculating flow on the side of a fast moving stream covering a range of mainstream Froude numbers varying from $Fr_o = 0.2$ to 4.5. Figure 1 shows the top view of the simulation problem and vorticity patterns on a horizontal x–y plane for several mainstream Froude numbers. Gravity is in the direction perpendicular to the plane. The depth and velocity of the mainstream are H_o and U_o, respectively, and the dimension of the square basin is L_b. At low Froude numbers, the roll-up of the vortex sheet across the mixing layer to form eddies determines the exchange process. The mixing at higher Froude numbers is affected by the radiation of the waves from the mixing layer and the waves in the recirculating flow.

We used a well-calibrated weighted essentially non-oscillatory (WENO) scheme to capture the shock waves while resolving turbulence in the mixing layer and the recirculating flow. Karimpour & Chu (2019) used this computational algorithm to examine the development of the free mixing layer between parallel streams. Their simulations were conducted for a range of convective Froude numbers, $Fr_c = (U_1 - U_2)/(c_1 + c_2) =$ 0.2 to 1.5, where U_1 and U_2 are the velocities and c_1 and c_2 the celerity of gravity waves in the free streams on the sides of the free mixing layer. Their results have shown that the shock waves hinder the growth of the mixing layer. The gas-dynamic studies by Papamoschou & Roshko (1988), Samimy & Elliott (1990) and Pantano & Sarkar (2002) for Mach numbers up to Ma_c = 1.1 have produced a similar reduction in the spreading rate of the free mixing layer between parallel air streams.

In the present simulation, tracer mass was introduced in the recirculating flow and monitored for its exchange with the mainstream during the simulation. The focus of the simulation was the determination of a retention time to compare with the laboratory measurements by Wang, Ghannadi & Chu (2010) and Wang (2015). The experiments by Wang *et al.* (2010) and Wang (2015) cover a range of Froude numbers varying from

$Fr_o = 0.2$ to 3.5. The paper has seven sections including this Introduction. Formulation of the shallow-water hydraulic model is given in § 2. Section 3 introduces a retention time to quantify the rate of the exchanges between the mainstream and the recirculating flow. The laboratory experiment and the correlation of a retention-time coefficient with the Froude number are given in § 4. A grid-refinement study is carried out in § 5 to determine the accuracy of the simulation. Section 6 shows the structure of the mixing layer and its interaction with the breaking shock waves within the recirculating flow. The final section contains the summary and conclusion.

2. Shallow-water hydraulic model

The numerical simulations for the exchanges were based on a shallow-water hydraulic model. The depth-averaged equations of the model are

$$\frac{\partial h}{\partial t} + \frac{\partial q_i}{\partial x_i} = 0, \tag{2.1}$$

$$\frac{\partial q_i}{\partial t} + \frac{\partial (u_j q_i)}{\partial x_j} = -gh\frac{\partial h}{\partial x_i} + ghS_i - \frac{c_f}{2}u_i\sqrt{u_j u_j} - \frac{1}{\rho}\left(\frac{\partial h\tau_{ij}}{\partial x_j}\right), \tag{2.2}$$

$$\frac{\partial ch}{\partial t} + \frac{\partial u_i ch}{\partial x_i} = 0, \tag{2.3}$$

where h is the depth of the flow, u_i are the velocity components in the x_i-directions, q_i is the flow rate, c is the tracer-mass concentration, c_f is the bottom friction factor, ρ is the density, and g is gravity. The indices are $i = 1, 2$ and $j = 1, 2$. The components of the velocity and discharge are $u_i = (u_x, u_y)$ and $q_i = (q_x, q_y)$ for the two-dimensional flow on the x–y plane. The channel slope $S_i = (S_o, 0)$ has only one component that is the longitudinal slope, S_o, in the x-direction. The repeated indices follow the tensor summation convention. We used the sub-grid-scale model by Vreman (2004) to conduct the large-eddy simulation of the turbulent flow. In this model, the sub-grid-scale stresses, τ_{ij}, and viscosity, ν_{sg}, are

$$\tau_{ij} = -2\nu_{sg}S_{ij} + \frac{1}{2}\delta_{ij}\tau_{kk} = -\nu_{sg}\left[\frac{\partial u_i}{\partial x_j} + \frac{\partial u_j}{\partial x_i}\right] + \frac{1}{2}\delta_{ij}\tau_{kk}, \tag{2.4}$$

$$\nu_{sg} = c\sqrt{\frac{B_\beta}{\alpha_{ij}\,\alpha_{ij}}}, \tag{2.5}$$

where

$$\alpha_{ij} = \frac{\partial u_j}{\partial x_i}, \quad \beta_{ij} = \Delta^2\,\alpha_{mi}\alpha_{mj} \quad \text{and} \quad B_\beta = \beta_{11}\,\beta_{22} - \beta_{12}^2. \tag{2.6}$$

The model constant $c = 2.5C_s^2$ and the value of the Smagorinsky constant is taken to be $C_s = 0.2$. The sub-grid scale filter size, Δ, is defined as $\Delta = \sqrt{\Delta x \Delta y}$. The coefficients in (2.6) were introduced by Vreman (2004) to ensure that the sub-grid viscosity is small in laminar and shear flows and is not as dissipative as the well-known Smagorinsky eddy viscosity. Our computational algorithm calculates α_{ij} first from the velocity field. It subsequently, calculates β_{ij}, and ultimately the value of B_β.

We used the fifth-order WENO scheme by Shu (2009) for the spatial interpolations. The logarithmic law of the wall is assumed for the velocity and discharge profiles near the basin's boundaries. The time integration of the equations was conducted using a fourth-order Runge–Kutta method. The numerical method and the validation of the

Case #	L_b (m)	c_f	U_o (m s^{-1})	H_o (m)	S_o (%)	Fr_o	$N = 1.0/\Delta x$
1	0.45	0.008	0.12838	0.042	0.016	0.20	200
2	0.45	0.008	0.25675	0.042	0.064	0.40	200
3	0.45	0.008	0.38513	0.042	0.144	0.60	200
4	0.45	0.008	0.51351	0.042	0.256	0.80	200
5	0.45	0.008	0.64189	0.042	0.400	1.00	200
6	0.45	0.008	0.96283	0.042	0.900	1.50	200
7	0.45	0.008	1.28378	0.042	1.600	2.00	200
8-1	0.45	0.008	1.60472	0.042	2.500	2.50	100
8-2	0.45	0.008	1.60472	0.042	2.500	2.50	200
8-3	0.45	0.008	1.60472	0.042	2.500	2.50	400
9	0.45	0.008	1.92566	0.042	3.600	3.00	200
10	0.45	0.008	2.05404	0.042	4.096	3.20	200
11	0.45	0.008	2.18242	0.042	4.624	3.40	200
12-1	0.45	0.008	2.24661	0.042	4.900	3.50	100
12-2	0.45	0.008	2.24661	0.042	4.900	3.50	200
12-3	0.45	0.008	2.24661	0.042	4.900	3.50	400
13	0.45	0.008	2.31080	0.042	5.184	3.60	200
14	0.45	0.008	2.43917	0.042	5.776	3.80	200
15	0.45	0.008	2.56755	0.042	6.400	4.00	200
16	0.45	0.008	2.88849	0.042	8.100	4.50	200

Table 1. Summary of parameters for numerical cases. Grid-refinement studies are performed for cases 8-1, 8-2, 8-3 and 12-1, 12-2, 12-3 for Fr_o = 2.5 and 3.5, respectively.

method for simulations of sub-critical and super-critical open-channel flow were given previously by Karimpour & Chu (2015).

The dimensions of the square basin are 0.45 m × 0.45 m and the basin is located 1.2 m downstream from the inlet of the main channel. The length and width of the open-channel main flow are 2.10 m and 3.00 m, respectively. The mesh sizes are $\Delta x = \Delta y = 0.005$ m. The depth of the main flow is $H_o = 0.042$ m. The bottom friction coefficient has a value of $c_f = 0.008$. The longitudinal slope, S_o, of the open channel was selected to produce the desirable velocity U_o and the Froude number, $Fr_o = U_o/\sqrt{gH_o}$, in the mainstream. The lateral slope of the channel is zero. Table 1 summarizes the parameters for 16 simulation cases and Froude numbers. The flow is uniform across the mainstream as it enters the computational domain. The outflow boundary condition is zero gradient. Figure 1 shows the vorticity profiles for three mainstream Froude numbers of (*a*) $Fr_o = 0.2$, (*b*) $Fr_o = 1.5$ and (*c*) $Fr_o = 3.0$. Waves were produced as the mainstream interacted with the recirculating flow in the square basin. For the cases of the super-critical mainstream as shown in (*b*,*c*), the mainstream was modified by oblique shock waves. The Froude lines with an angle of $\theta = \sin^{-1}(1/Fr_o)$ in the figure mark the location of the oblique shock waves separating the undisturbed mainstream from the flow exchanging with the recirculating flow in the basin. The waves and turbulence produced by the exchange is complex but the overall exchange can be defined by a retention time as explained in the subsequent section.

3. Retention time

The retention time, τ, is a time scale introduced to characterize the exchange of the tracer mass in the recirculating flow with its external mainstream. It is defined by the

fractional-rate equation as follows:

$$\frac{1}{\bar{c}}\frac{\mathrm{d}\bar{c}}{\mathrm{d}t} = \frac{1}{\tau}, \tag{3.1}$$

where $\bar{c}$ is an average of tracer-mass concentration over an area in the recirculating flow. The solution to the fractional-rate equation is

$$\ln\left(\frac{\bar{c}}{c_o}\right) = \left(-\frac{t}{\tau}\right). \tag{3.2}$$

Booij (1989) used this retention time to characterize the exchange between a recirculating flow in a square basin and a sub-critical mainstream. The dimensionless parameter corresponding to retention time is the retention-time coefficient

$$C_\tau = \frac{\tau U_o}{L_b}. \tag{3.3}$$

In the present simulation, tracer mass of uniform concentration, c_o, was specified over the entire square basin at a time $t = t_1$, when the recirculating flow had reached the quasi-steady state. Figures 2(*a*), 2(*b*) and 2(*c*) show the subsequent instantaneous tracer-mass concentration distribution, $c(x, y, t)$, for the mainstream Froude numbers of $Fr_o = 0.2, 3.2$ and 3.8, respectively. The development of a mixing layer between the mainstream and the recirculating flow in the basin is responsible for the tracer-mass exchange. The entrainment of the fluids from two sides of the mixing layer led to the exchanges that caused the depletion of tracer mass in the basin. Figure 2(*d*) shows the basin-average dye concentration, $\bar{c}/c_o$, and its reduction with time, $(t - t_1)U_o/L_b$, on a semi-logarithmic scale for these three mainstream Froude numbers. Reduction in concentration with time perfectly matches the solution of the fractional-rate equation, (3.2). The retention-time coefficient, C_τ, was determined as the inverse slope of the straight lines, marked in the semi-logarithmic plots. This slope was maintained despite several orders of magnitude reduction in tracer-mass concentration, $\bar{c}/c_o$.

Figure 2(*d*) demonstrates that the retention time is a unique parameter that can be identified for any Froude number. The values of the retention-time coefficient as defined by the inverse slopes of the lines in figure 2(*d*) are

$$C_\tau = 32, \quad \text{for } Fr_o = 0.2, \tag{3.4}$$

$$C_\tau = 134, \quad \text{for } Fr_o = 3.2, \tag{3.5}$$

$$C_\tau = 55, \quad \text{for } Fr_o = 3.8. \tag{3.6}$$

This variation of the retention time with the Froude number is not monotonic. The retention-time coefficient increased from $C_\tau = 32$ to 134 from $Fr_o = 0.2$ to 3.2, and then dropped sharply from $C_\tau = 134$ to 55 as the Froude number varied only slightly from $Fr_o = 3.2$ to 3.8.

The value of the retention-time coefficient, $C_\tau = 32$, for the sub-critical mainstream Froude number of $Fr_o = 0.2$ was in agreement with the laboratory measurements by Booij (1989) and Altai & Chu (1997). The significant increase in the retention-time coefficient between $Fr_o = 0.2$ and 3.2, by more than a factor of 4 from $C_\tau = 32$ to 134, is associated with the suppression of mixing-layer growth which, according to Karimpour & Chu (2019), is due to the radiation of waves from the mixing layer. This suppression of the mixing-layer growth is consistent with the analogous study in gas dynamics by Pantano & Sarkar (2002). Figure 2(*d*) also shows a sharp drop in the retention-time coefficient from

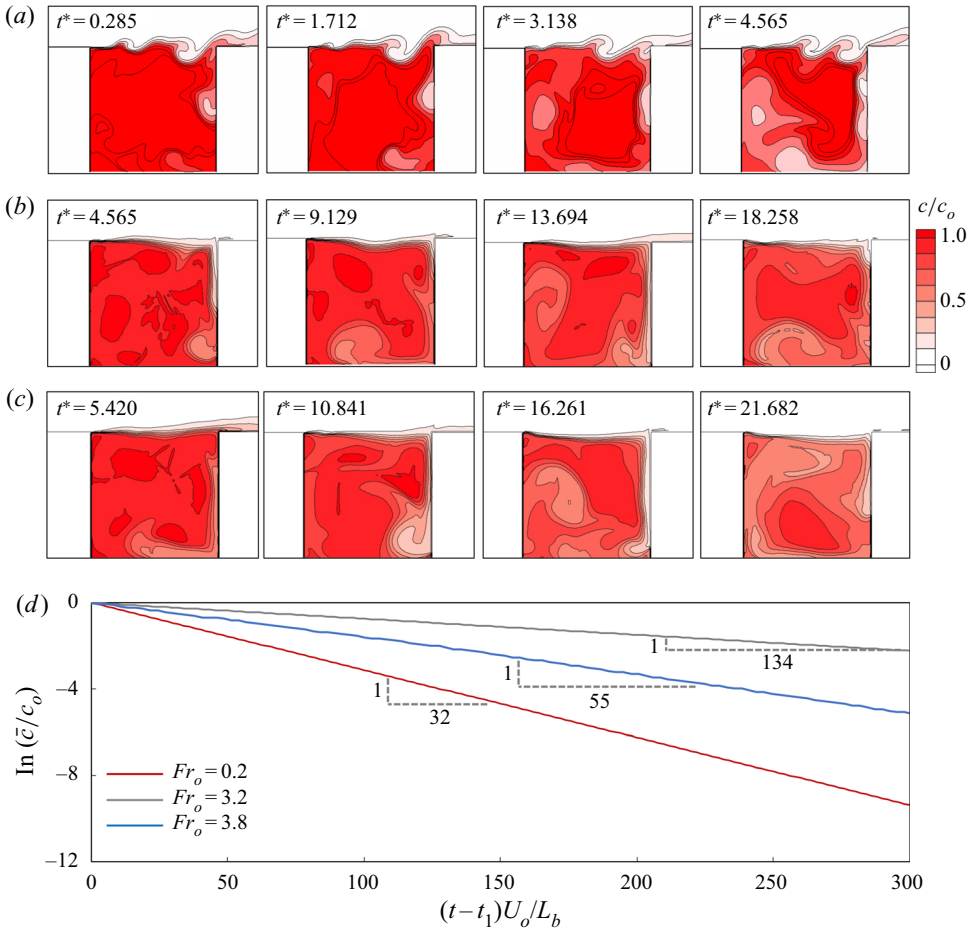

Figure 2. Sequence of images for the c/c_o distribution in the recirculating flow in the square basin for (*a*) $Fr_o = 0.2$, (*b*) $Fr_o = 3.2$ and (*c*) $Fr_o = 3.8$. (*d*) The average of the dye concentration over the square basin, $\bar{c}/c_o$, obtained from numerical simulation, and its reduction with the dimensionless time, $t^* = (t - t_1)U_o/L_b$, on a semi-logarithmic scale for $Fr_o = 0.2$, 3.2 and 3.8. Here, t_1 is the onset of quasi-steady state mixing and is when the tracer is introduced into the basin and c_o is the initial tracer concentration at t_1.

$Fr_o = 3.2$ to 3.8. This drop cannot be explained by the suppression of growth in the mixing layer. The interaction of the mixing layer with the shock waves in the side basin affects the retention-time coefficient. The explanation of this sharp drop will be given later in § 6.

Figure 3 shows the dependence of the retention-time coefficient, C_τ, on the mainstream Froude number Fr_o and the comparison of simulation results with the laboratory measurements. The retention-time coefficient increases with the Froude number from a value of $C_\tau = 32$ at $Fr_o = 0.2$ to a value of $C_\tau = 134$ at $Fr_o = 3.2$. These simulation results over the range of $Fr_o = 0.2$ to 3.0 are in support of the laboratory experiments by Wang *et al.* (2010) and Wang (2015). But the most remarkable result shown in figure 3 is the 'sharp drop' in value of the retention-time coefficient from the value of $C_\tau = 134$ at $Fr_o = 3.2$ to a value of $C_\tau = 60$ at $Fr_o = 3.4$.

The irregularities in the increasing retention-time coefficient part in figure 3 cannot be attributed to computational inaccuracies. These are believed to be associated with the waves in the basin and their interactions with the mixing layer. The review paper by

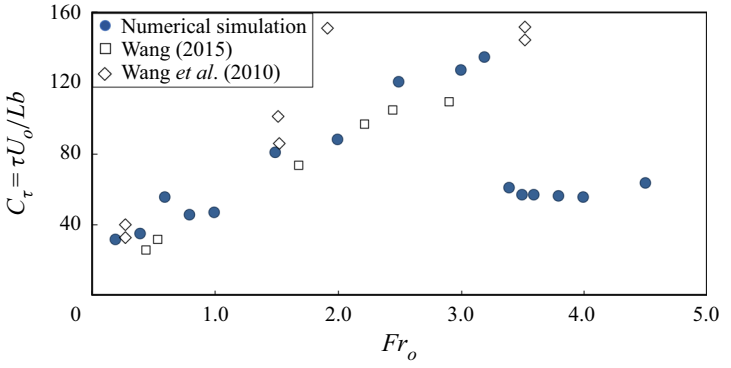

Figure 3. Non-monotonic variations of the retention-time coefficient, $C_\tau = \tau U_o/L_b$, with the mainstream Froude number, Fr_o. The simulation results, denoted by the solid symbols, cover a range of Froude numbers varying from $Fr_o = 0.2$ to 4.5. The laboratory measurements by Wang *et al.* (2010) and Wang (2015), denoted by the open symbols, cover a smaller range of Froude numbers from $Fr_o = 0.2$ to 3.5.

Rockwell & Naudascher (1978) has provided discussions on such interactions at low Mach numbers.

4. Comparison with laboratory experiments

Two sets of experimental data are presented in figure 3 that were obtained from two different experimental facilities. The experimental set-ups are illustrated in detail in Wang *et al.* (2010) and Wang (2015). The retention-time coefficients obtained in the first series of experiments by Wang *et al.* (2010), denoted by the open-diamond symbols in the figure, were generally higher than the coefficients obtained by the numerical simulation. The coefficients obtained in the later series of experiments by Wang (2015), denoted by the open-square symbols, however, were lower in value than the numerical results. The experiments by Wang *et al.* (2010) were conducted a number of years earlier in a different facility from the experiments conducted later by Wang (2015).

The earlier experiments by Wang *et al.* (2010) were conducted in a 142 cm wide channel. The dimensions of the basin on the side were 15 cm × 15 cm and the basin was located immediately after the entrance to the main channel. The retention time was determined in the earlier experiments based on the average of the tracer-mass concentration over a small central region, $\bar{c}_c$. Figure 4 shows the small central region in the basin that was used to determine the average concentration, $\bar{c}_c$. The retention-time coefficient was determined by curve fitting the data with (3.2). In these experiments, rhodamine red dye was introduced into the basin with an initial concentration c_o and a dye flow rate q_o for a period of time until the concentration in the basin had reached a quasi-steady state. The concentration of the red dye was determined using the video imaging method developed by Zhang & Chu (2003) and Chu, Liu & Altai (2004). The presence of the red dye in the basin reduced the intensity of the green light. The percentage of the green-light intensity reduction was used to determine the dye concentration. The data denoted by the open symbols in the figure were the dimensionless concentration, $\bar{c}_c U_o L_b H/c_o q_o$, for an experiment with a mainstream Froude number of $Fr_o = 3.5$. The dashed line is (3.2) for $C_\tau = 145$ that best fit the experimental data.

The later experiments by Wang (2015) were conducted in a smaller channel. The width of the small channel was only 35.5 cm. The basin dimension for the smaller facility was 24 cm × 24 cm. The retention time was determined in the later experiment based on the

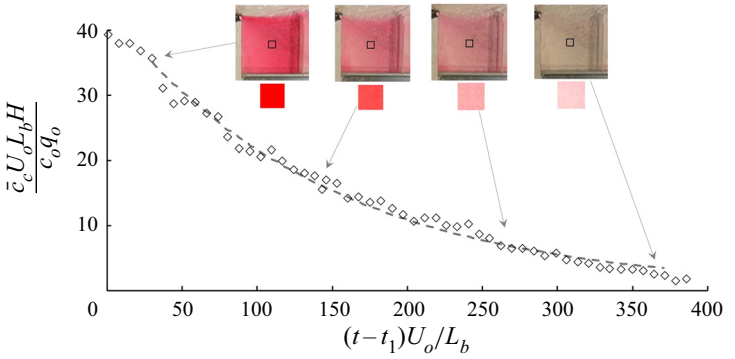

Figure 4. The determination of the retention-time coefficient in the laboratory experiment by Wang *et al.* (2010) for $Fr_o = 3.5$. The average concentration, $\bar{c}_c$, was obtained in the central region of the basin marked by the square symbols. The dashed line is the (3.2) for $C_\tau = 145$ that fits the experimental data.

average of the tracer-mass concentration over the entire basin, $\bar{c}$. The super-critical flow was produced using a sluice gate in this facility. In the super-critical range, large surface waves were produced by the edges of the sluice gate. The disturbances caused by the surface waves in the narrow main channel produced great penetration to the mixing layer. This might have caused the retention-time coefficient obtained in the experiments by Wang (2015) to be slightly lower than the results of the numerical simulation.

Furthermore, Wang *et al.* (2010) obtained the retention-time coefficient using the concentration averaged over a small area in the core region of the recirculating flow. The entrapment of the tracer dye in the core region is more persistent than in the outer region. This explains further why the retention-time coefficients, C_τ, obtained by Wang *et al.* (2010) were generally higher than those in the numerical simulation. Despite the difference in the experimental set-ups, both experiments produced retention-time coefficients that follow a similar trend of dependence on the mainstream Froude number, Fr_o, as the trend of dependence in the simulation, up to a Froude number of approximately $Fr_o \simeq 3.0$.

In both experiments, the dye concentration was estimated based on a calibration curve. Red dye of known concentration was placed in a calibration box. The calibration curve is a relationship between the reduction of green-light intensity in the video image and the known dye concentrations. This video imaging method is affected by the presence of surface waves. For super-critical flow of high Froude number, the amplitude of the wave was comparable to the water depth and the accuracy of the video imaging is compromised. To compensate for the wave's effect, an artificial disturbance was introduced to the water in the calibration box. Such an artificial disturbance in the box cannot perfectly replicate the surface waves in the square basin at large Froude numbers. We believe that this has partly contributed to discrepancies between numerical simulations and laboratory measurements.

We have experienced difficulties of measuring the dye concentration at high Froude numbers. The free-surface waves that obscured the incident and reflected light beams were very large in amplitude for Froude numbers greater than 3.5. For this reason, Wang (2015) and Wang *et al.* (2010) did not report any experimental data beyond $Fr_o = 3.5$.

5. Grid-refinement study

To corroborate the unexpected result, we conducted a grid-refinement study for a Froude number $Fr_o = 2.5$, before the sharp drop in value of the retention-time coefficient,

$Fr_o = 3.5$				$Fr_o = 2.5$			
$N = 1.0/\Delta x$	$\tau U_o/L_b$	Order (P)	FE (%)	$N = 1.0/\Delta x$	$\tau U_o/L_b$	Order (P)	FE (%)
100	80.6323	—	42.16	100	181.7637	—	53.53
200	57.4530	2.53	1.29	200	119.35	2.939	0.87
400	56.8483	—	0.22	400	118.4510	—	0.11

Table 2. The mesh-refinement study for the accuracy and order of convergence conducted for the two mainstream Froude numbers of $Fr_o = 2.5$ (cases 8-1, 8-2 and 8-3) and 3.5 (cases 12-1, 12-2 and 12-3) before and after the 'sharp drop' in the value of $\tau U_o/L_b$.

and at Froude number $Fr_o = 3.5$, immediately after the drop. The refinement ratio, the corresponding retention coefficient, the order of convergence (P) and the fractional error (FE) are presented in table 2. The convergent values, as defined by Karimpour & Chu (2015), were for $\tau U_o/L_b = 56.85$ and 118.5 at $Fr_o = 3.5$ and 2.5, respectively. The respective fractional error and order of convergence were FE(%) = 0.22 and 0.11, and P = 2.5 and 2.9. The grid-refinement study not only established the accuracy of the numerical simulation, it also ascertained the existence of the sharp drop in value of the retention-time coefficient from $C_\tau = \tau U_o/L_b = 118$ to 57 across the changes in Froude number from $Fr_o = 2.5$ to 3.5. The simulation results presented in figure 3 were obtained using $N = 1.0/\Delta x = 200$ nodal points.

6. Discussion

We have shown how the retention time is a uniquely defined parameter that characterizes the exchange between the recirculating flow and the mainstream. The retention-time coefficient increased from a value of $C_\tau \simeq 32$ at $Fr_o = 0.2$ to a value of $C_\tau \simeq 134$ at $Fr_o = 3.2$. This then was followed by a 'sharp drop' to the value of $C_\tau \simeq 61$ at $Fr_o = 3.4$. This striking variation of the retention-time coefficient with the mainstream Froude number shown in figure 3 is associated with structural changes in the mixing layer and the recirculating flow as explained in the following sub-sections.

6.1. *The mixing layer between the mainstream and the recirculating flow*

The vorticity and the tracer-mass concentration profiles in figures 1 and 2 delineate the structural dependence of the flow on the mainstream Froude number. The sub-critical exchanges at $Fr_o = 0.2$, as shown in figures 1(*a*) and 2(*a*), were associated with the coherent eddies in the mixing layer. The eddies coalesced to form bigger eddies in the mixing layer as the fluid was drawn into the mixing layer through a process known as entrainment, from the mainstream on one side and from the recirculating flow in the basin on the other side.

Studies of free mixing layers between parallel streams by Karimpour & Chu (2019) and Pantano & Sarkar (2002) have found that the spreading rate is reduced by the radiation of waves from the mixing layers. Similar effect on the spreading rate may occur in the mixing layer between the mainstream and the recirculating flow and this may explain the consistent increase in the retention-time coefficient with the mainstream Froude number from $Fr_o = 0.2$ to 3.2.

The lateral spreading of the mixing layer is affected by the wave radiation from the mixing layer. With radiation of the wave energy, less energy is available for the

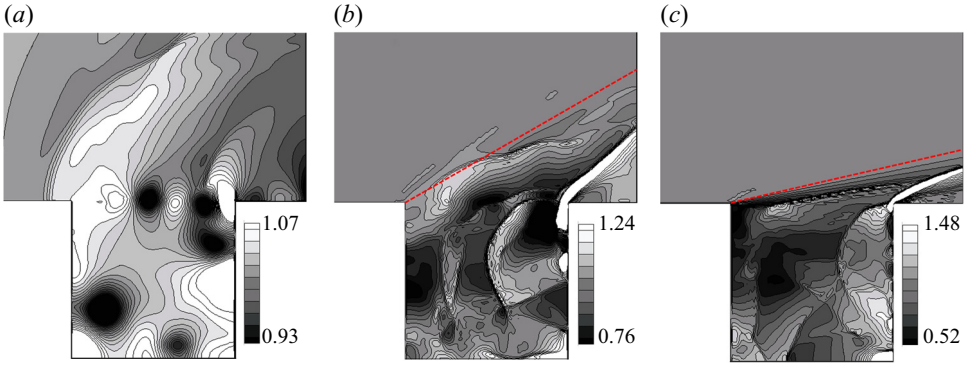

Figure 5. The eddies and waves as defined by the depth h/H for the mainstreams with (*a*) $Fr_o = 0.2$, (*b*) $Fr_o = 2.0$ and (*c*) $Fr_o = 4.5$. The red dashed lines in (*b*,*c*) are the 'Froude lines' separating the undisturbed mainstream from exchange flow with the recirculating flow in the basin.

production of turbulence in the mixing layer. The mixing layers of higher Froude numbers were relatively less energetic and, therefore, made less contribution to the exchange processes. The suppression of turbulence in the mixing layer can explain the increase in the retention-time coefficient with the mainstream Froude number. This, however, cannot explain the 'sharp drop' in value of the retention-time coefficient from $Fr_o = 3.2$ to $Fr_o = 3.4$.

6.2. *The occurrence of shock waves within the recirculating flow*

The contours of the relative depth, h/H_o, in figures 5(*a*), 5(*b*), and 5(*c*) delineate further the interaction between the eddies and waves for the cases with the mainstream Froude numbers $Fr_o = 0.2$, 1.5 and 4.5, respectively. For the sub-critical flow with $Fr_o = 0.2$, the depth fluctuations in the range of $h/H_o \simeq 1 \pm 0.07$ were quite small. The depth fluctuations increased with the Froude number to $h/H_o \simeq 1 \pm 0.24$ for $Fr_o = 2.0$ and then to $h/H_o \simeq 1 \pm 0.48$ for $Fr_o = 4.5$. For the mainstream with the large Froude number of $Fr_o = 4.5$, shock waves of significant amplitude were observed to occur within the recirculating flow in the basin. The wave height of the shock waves, $(h_{max} - h_{min})/H_o \simeq 0.96$, in this case was comparable to the mean depth.

The 'sharp drop' in retention-time coefficient was associated with a major structural change in the recirculating flow. We examine this structural change in figures 6(*a*) and 6(*b*) using the local Froude number $Fr = \sqrt{u^2 + v^2}/\sqrt{gh}$ as the indicator. The distinction between flow shown in figure 6(*a*) with the mainstream Froude number of $Fr_o = 2.0$ and the flow shown in figure 6(*b*) of $Fr_o = 4.5$ is the formation of shock waves inside the basin. The red colour in the contours defines the area where the local Froude number is $Fr > 1$. The blue colour, on the other hand, defines the area where the local Froude number is $Fr < 1$. The change in blue to red defines the front of the shock waves in this figure.

The recirculating flow in case (*a*) with a $Fr_o = 2.0$, had a nearly stagnant core. The local Froude number in the core defined by the blue colour is nearly zero. The tracer mass entrapped in the stagnant core was not accessible for exchange across the mixing layer. The circulation mainly around the edge of the basin was relatively steady with fewer waves in the circulation.

The velocity of the recirculating flow was much higher in case (*b*) with $Fr_o = 4.5$. The local Froude number is rapidly changing from the sub-critical (blue) to super-critical (red). Shock waves of large amplitude were observed contributing to mixing throughout the entire basin. The large-amplitude shock waves in the basin and their interaction with

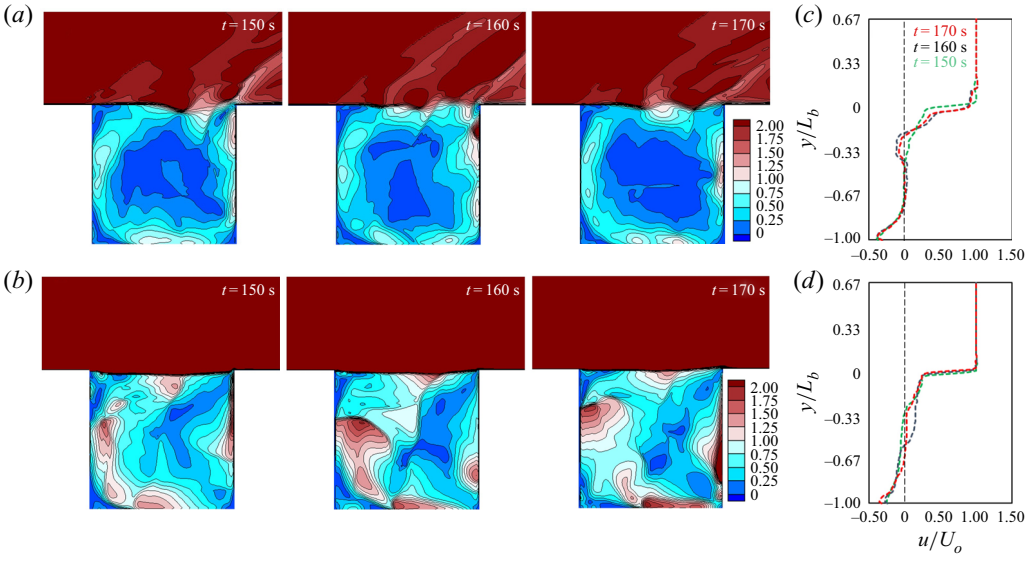

Figure 6. The wave dynamics in the recirculating flow as delineated by the local Froude number $Fr = \sqrt{u^2 + v^2}/\sqrt{gh}$ shown at 10 s intervals, (*a*) for Fr_o = 2.0 before the sharp drop and (*b*) for $Fr_o = 4.5$ after the sharp drop. The corresponding velocity profile for u/U_o across the flow at the mid-section ($x = L_b/2$) is in (*c*,*d*).

the mixing layer promoted the exchanges leading to the sharp drop in the value of the retention-time coefficient at $Fr_o = 3.4$ (between the $Fr_o = 2.0$ and 4.5).

The magnitude of the recirculating velocity in the basin was approximately equal to one third of the mainstream velocity, U_o, as shown in figures 6(*c*) and 6(*d*) for mainstream Froude numbers of Fr_o = 2.0 and 4.5. Therefore, the local Froude number in the recirculating area would begin to exceed the critical value of unity when the mainstream Froude number exceeds $Fr_o \simeq 3.0$. The interaction of these shock waves in the basin with the mixing layer is believed to be the reason for the sudden increase in the exchange and the sharp drop in the value of retention-time coefficient at the mainstream Froude number of approximately $Fr_o = 3.4$.

7. Summary and conclusion

We conducted numerical simulations of the recirculating flow in a square basin using a shallow-water hydraulic model for a range of mainstream Froude numbers varying from $Fr_o = 0.2$ to 4.5. A retention-time coefficient was introduced to characterize the exchange of mass across the mixing layer. Two distinct ranges of dependence on Froude number have been observed: (i) the value of the retention-time coefficient increased with the Froude number over the range of $Fr_o = 0.2$ to 3.2, and (ii) a sharp drop in the value of the coefficient occurred at a Froude number of $Fr_o \simeq 3.4$. The increase in values of the retention-time coefficient over the range of $Fr_o = 0.2$ to 3.2 is due to the suppression of turbulence production in the mixing layer. The sharp drop, on the other hand, is associated with the formation of shock waves within the recirculating flow in the basin and the interaction of these shock waves with the mixing layer. The laboratory observation is consistent with the numerical simulations in the range of Froude number from Fr_o= 0.2 to 3.0.

This is the first study highlighting the role of shock waves within a recirculating flow on the exchange process with the mainstream. Geometrical variations of the basin produced by the length-to-width ratio, the change in depth within the basin and the existence of adjacent basins, have effects on the exchange processes and the sudden drop in the retention-time coefficient. The role of these variations has been studied in subcritical flows by Uijttewaal *et al.* (2001). Further studies are required to investigate their role in the exchange process for supercritical flows of high Froude numbers.

The shallow-water hydraulic model had reproduced the flow at low mainstream Froude number when the exchange was governed by the production of coherent eddies and roll-up of the vortex sheet in the mixing layer. The model was also capable of producing the waves when the exchange process was affected by the shock waves in the basin. The success of the numerical simulations for the high-speed shear flow is attributable to the reliable shock capture schemes developed by Karimpour & Chu (2015) for the numerical simulations. Karimpour & Chu (2014) used this shallow-water hydraulic model to find the lateral discharge from a side weir in an open-channel flow. Their results produced discharge coefficients in perfect agreement with those of laboratory experiments. Karimpour & Chu (2016, 2019) studied the role of waves on the development of the free mixing layer using the same computational algorithm. Their results for open-channel flow were validated by the observations made in the analogous gas-dynamic problem. The present simulation is an additional piece of evidence supporting the general use of the model for simulation of shallow shear flows over a wide range of Froude numbers.

Declaration of interests. The authors report no conflict of interest.

Author ORCIDs.
Shooka Karimpour https://orcid.org/0000-0002-3229-749X.

References

Alavian, V. & Chu, V.H. 1985 Turbulent exchange flow in shallow compound channel. In *Proceedings of the 21st International Congress of IAHR*, pp. 446–451.

Altai, W. & Chu, V.H. 1997 Retention time in recirculating flow. In *Environmental and Coastal Hydraulics: Protecting the Aquatic Habitat*, pp. 9–14. ASCE.

Babarutsi, S., Ganoulis, J. & Chu, V.H. 1989 Experimental investigation of shallow recirculating flows. *ASCE J. Hydraul. Engng* **115** (7), 906–924.

Booij, R. 1989 Exchange of mass in harbours. In *Proceedings of 23rd IAHR Congress*.

Chu, V.H., Liu, F. & Altai, W. 2004 Friction and confinement effects on a shallow recirculating flow. *J. Environ. Engng Sci.* **3** (5), 463–475.

Karimpour, S. & Chu, V.H. 2014 Transverse dam-break waves. *J. Fluid Mech.* **758**, R2.

Karimpour, S. & Chu, V.H. 2015 High-order interpolation schemes for shear instability simulations. *Intl J. Numer. Meth. Heat Fluid Flow* **25** (6), 1340–1360.

Karimpour, S. & Chu, V.H. 2016 Instability of unbounded transverse mixing layer in shallow waters. *Can. J. Civ. Engng* **43** (6), 504–510.

Karimpour, S. & Chu, V.H. 2019 The role of waves on mixing in shallow waters. *Can. J. Civ. Engng* **46** (2), 134–147.

Kvočka, D., Ahmadian, R. & Falconer, R.A. 2017 Flood inundation modelling of flash floods in steep river basins and catchments. *Water* **9** (9), 705.

McCoy, A., Constantinescu, G. & Weber, L.J. 2008 Numerical investigation of flow hydrodynamics in a channel with a series of groynes. *ASCE J. Hydraul. Engng* **134** (2), 157–172.

Pantano, C. & Sarkar, S. 2002 A study of compressibility effects in the high-speed turbulent shear layer using direct simulation. *J. Fluid Mech.* **451**, 329.

Papamoschou, D. & Roshko, A. 1988 The compressible turbulent shear layer: an experimental study. *J. Fluid Mech.* **197**, 453–477.

Petaccia, G., Natale, L., Savi, F., Velickovic, M., Zech, Y. & Soares-Fraz ao, S. 2013 Flood wave propagation in steep mountain rivers. *J. Hydroinform.* **15** (1), 120–137.

ROCKWELL, D. & NAUDASCHER, E. 1978 Review – self-sustaining oscillations of flow past cavities. *Trans. ASME J. Fluids Engng* **100** (2), 152–165.

SAMIMY, M. & ELLIOTT, G.S. 1990 Effects of compressibility on the characteristics of free shear layers. *AIAA J.* **28** (3), 439–445.

SHIELDS, F.D., COOPER, C.M. & KNIGHT, S.S. 1995 Experiment in stream restoration. *ASCE J. Hydraul. Engng* **121** (6), 494–502.

SHU, C.-W. 2009 High order weighted essentially nonoscillatory schemes for convection dominated problems. *SIAM Rev.* **51** (1), 82–126.

UIJTTEWAAL, W.S.J., LEHMANN, D.V. & VAN MAZIJK, A. 2001 Exchange processes between a river and its groyne fields: model experiments. *ASCE J. Hydraul. Engng* **127** (11), 928–936.

UIJTTEWAAL, W.S. 2005 Effects of groyne layout on the flow in groyne fields: laboratory experiments. *ASCE J. Hydraul. Engng* **131** (9), 782–791.

VAN PROOIJEN, B.C., BATTJES, J.A. & UIJTTEWAAL, W.S.J. 2005 Momentum exchange in straight uniform compound channel flow. *ASCE J. Hydraul. Engng* **131** (3), 175–183.

VREMAN, A.W. 2004 An eddy-viscosity subgrid-scale model for turbulent shear flow: algebraic theory and applications. *Phys. Fluids* **16** (10), 3670–3681.

WANG, T. 2015 Subcritical and supercritical shear flows in shallow waters-numerical simulations and laboratory experiments. PhD thesis, McGill University.

WANG, T., GHANNADI, S.K. & CHU, V.H. 2010 Retention of dye tracer in side basins exchanging with subcritical and supercritical flows. *River Flow* **2010**, 1775–1782.

XIANG, K., YANG, Z., WU, S., GAO, W., LI, D. & LI, Q. 2020 Flow hydrodynamics of the mixing layer in consecutive vegetated groyne fields. *Phys. Fluids* **32** (6), 065110.

YOSSEF, M.F.M. & DE VRIEND, H.J. 2010 Sediment exchange between a river and its groyne fields: mobile-bed experiment. *ASCE J. Hydraul. Engng* **136** (9), 610–625.

ZHANG, J.-B. & CHU, V.H. 2003 Shallow turbulent flows by video imaging method. *J. Engng Mech. ASCE* **129** (10), 1164–1172.